Journal of Electromagnetic Waves and Applications

ISSN: 0920-5071 (Print) 1569-3937 (Online) Journal homepage: https://www.tandfonline.com/loi/tewa20

A compact slot MIMO antenna for smartphones with metal housing

Di Wu, Xiaoxue Hua, Sing Wai Cheung, Bo Wang, Min Li & Bing Xiao

To cite this article: Di Wu, Xiaoxue Hua, Sing Wai Cheung, Bo Wang, Min Li & Bing Xiao (2018) A compact slot MIMO antenna for smartphones with metal housing, Journal of Electromagnetic Waves and Applications, 32:2, 204-214, DOI: 10.1080/09205071.2017.1374883

To link to this article: https://doi.org/10.1080/09205071.2017.1374883

JOURNAL OF ELECTROMAGNETIC WAVES AND APPLICATIONS, 2018
VOL. 32, NO. 2, 204–214
https://doi.org/10.1080/09205071.2017.1374883

Taylor & Francis
Taylor & Francis Group

A compact slot MIMO antenna for smartphones with metal housing

Di Wu, Xiaoxue Hua, Sing Wai Cheung, Bo Wang, Min Li and Bing Xiao

Department of Electrical and Electronic Engineering, The University of Hong Kong, Hong Kong, China

ABSTRACT

A compact slot multiple-input multiple-output Antenna (CSMA) for smartphones with metal housing is proposed in this paper. The antenna has a slot radiator shared between two input ports and a T-shaped defect-ground slot (DGS) for decoupling. A function for selecting the best dimensions of the DGS for optimum decoupling is derived using the transmission theory. The CSMA antenna is designed using simulation to operate in the 2.4-GHz wireless-area-network (WLAN) system and then fabricated for measurement. Measured results show that the antenna has an impedance bandwidth (IMBW) of 2.4–2.48 GHz, mutual coupling from −19 to −29 dB and envelope-correlation coefficient (ECC) below 0.0867 within the IMBW. The antenna is very easy to fabricate and is a potential candidate for the MIMO smartphones antennas with metal housing.

ARTICLE HISTORY
Received 6 June 2017
Accepted 25 August 2017

KEYWORDS
Mobile antenna; metal housing; multiple-input multiple-output antenna; slot antenna

1. Introduction

In recent years, an increasing number of smartphones manufacturers prefer to use metal housing in their flagship products. Metal housing can improve the rigidity and strength of the mobile handsets, and has adorable metal appearances for the consumers. For smartphones with metal housing, traditional mobile antennas like inverted-F antennas (IFAs), monopole, or loop antennas seem to be difficult to be used. Therefore, some innovative techniques such as metal-rim antennas [1,2], slots [3], and open slot antennas [4,5] have been proposed. These techniques also help reduce the manufacturing costs, as no additional antenna is required.

Multiple-input multiple-output (MIMO) technology is one of the core technologies for the current 4G and future 5G wireless standards. To increase isolation of antenna elements in MIMO antennas for mobile applications, different decoupling techniques such as neutralization-line techniques [6], LC decoupling networks [7], T-shaped protruded ground [8], ground resonator [9], and cutting slots on ground planes [10,11] have been reported. However, these decoupling techniques [6–11] are difficult to be integrated with the metal housing of smartphones. In [12], a two-port sharing the same slot antenna with a simple slot for decoupling was designed using the complementary layout of a two-port dipole antenna and based on the Babinet's Principle [13]. With the two-port dipole designed to achieve low mutual decoupling, the

CONTACT Bo Wang bowang@eee.hku.hk

two-port slot antenna could also achieve low mutual decoupling. However, the method could not be used to directly design the slot antenna and there was no mention about how the two-port dipole with low coupling was designed. Moreover, the long defect ground slot (DGS) would take too much space if used on the metal housing of smartphones.

In this paper, a compact slot MIMO antenna (CSMA) is proposed for smartphones with metal housing. The two antenna elements of the CSMA and its decoupling structure are achieved using only one slot structure. Hence, comparing to other MIMO antennas [4–11], the proposed CSMA is very compact, as there is no distance between the two antenna elements. To the best knowledge of the authors, the proposed CSMA has never been used to design MIMO antennas on metal housing. The antenna is etched on the metal housing, so it is very easy to be fabricated and helps reduce the manufacturing cost. The EM simulation tool CST is used to study the CSMA. For verification, the antenna is fabricated and measured using the antenna measurement equipment, the Satimo SG24 system. The antenna has an excellent MIMO performance.

2. Antenna design

The geometry of the proposed CSMA for smartphones with metal housing is shown in Figure 1. In our study, the metal housing of a smartphone is modeled using a metal cover with a size of $L_g \times W_g = 120 \times 60$ mm^2 and a metal rim with a width of w1 = 5 mm. The CSMA consists of a sharing straight slot as the radiator and a T-shaped DGS for decoupling, with both etched on a metal cover, as shown in Figure 1(a). The size of the slot radiator is ls × ws = 44.3 × 2 mm^2, where the length ls is equivalent to about $\lambda_g/2$, with λ_g being the guide wavelength at 2.45 GHz in the WLAN band. The T-shaped DGS, as shown in Figure 1(b), consists of a horizontal slot with a length of $l_d = 34$ mm and a vertical slot with a length of $l_g = 4$ mm. The width of the T-shaped DGS is $w_d = 1$ mm. The metal cover is printed on a Rogers substrate, RO4350B, with a thickness of 0.8 mm, a relative permittivity of 3.48 and a loss tangent of 0.0037. Two 50-Ω micro-strip lines, serving as two input ports, are printed on the bottom layer of the substrate to coupled-feed the slot radiator. The distance $l_1 = 4$ mm and the extended length lm = 2 mm are used for good impedance matching to the slot radiator. It should be noted that, as the main antenna (2G/3G/4G) needs to be placed at the bottom side of the mobile phone, the CSMA should be placed at the top side of the phone to reduce interaction between the main antenna and the CSMA (WIFI-MIMO) antenna. In addition, placing the CSMA at the top side also helps to reduce the human hand effects. Detailed dimensions of the design are listed in Table 1, which are used to fabricate the prototyped antenna shown in Figure 2.

3. Decoupling analysis

Mutual decoupling of the CSMA is analyzed using the transmission line theory as follows. The equivalent transmission-line model of the CSMA is shown in Figure 3, where the two

Table 1. Dimensions of proposed antenna (mm).

L_g	W_g	d	t_1	l_f	w_f	w_1
120	60	32.82	0.76	10	1.74	5
w_d	w_s	l_d	l_m	l_1	l_s	l_g
1	2	34	2	4	44.3	4

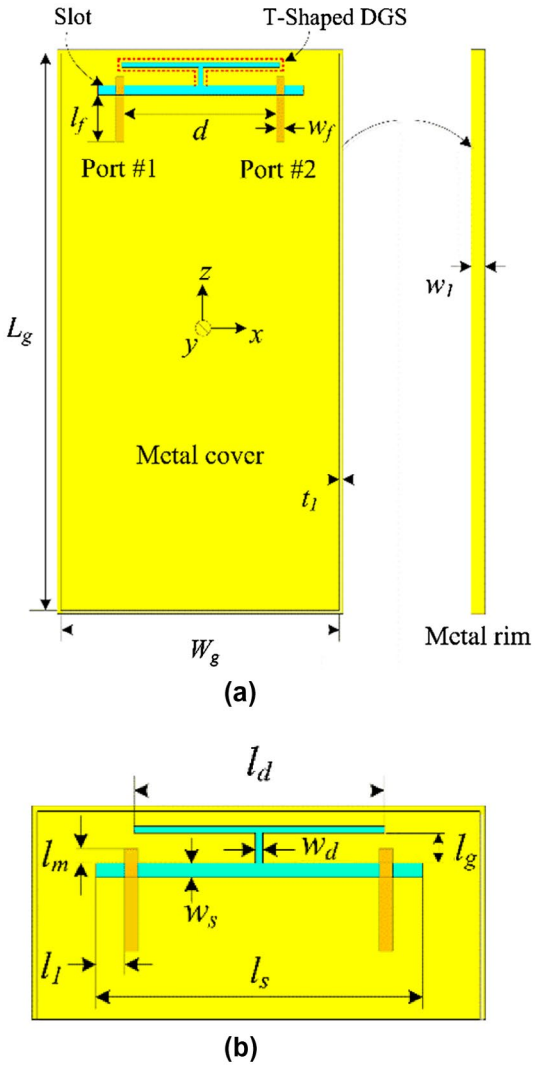

Figure 1. Geometry and dimensions of proposed CSMA antenna: (a) on a standard PCB, and (b) enlarged view (top layer, Rogers 4350B substrate, and bottom layer).

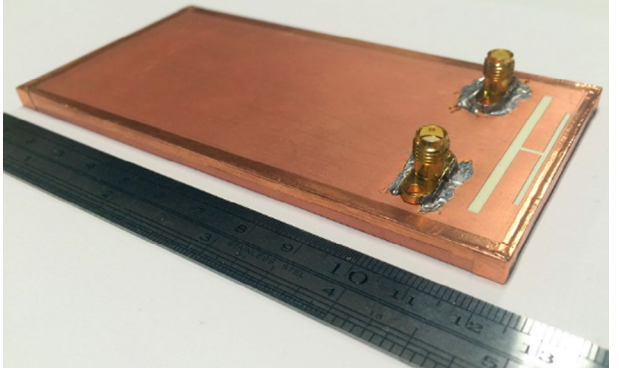

Figure 2. Prototyped antenna.

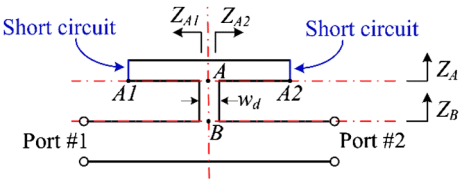

Figure 3. Equivalent transmission line model of the proposed CSMA.

ends, denoted as *A*1 and *A*2, of the DGS is short circuited. The input impedances, denoted as Z_{A1} and Z_{A2}, looking from point *A* into the *A*1 and *A*2 directions can be written as [14]

$$Z_{A1} = Z_{A2} = jZ_0 \tan \beta(l_d/2) \tag{1}$$

where Z_0 is the characteristic impedance of the transmission line of the DGS and β is the wavenumber given by:

$$\beta = 2\pi/\lambda_g \tag{2}$$

where λ_g is the guide wavelength at 2.45 GHz.

In the transmission model of Figure 3, the signal propagating from point B to point *A* will see the transmission lines *A*-*A*1 and *A*-*A*2 in parallel, so the input impedance Z_A at point *A* is

$$Z_A = 1/Y_A = 1/\left(1/Z_{A1} + 1/Z_{A2}\right) = \frac{jZ_0 \tan \beta(l_d/2)}{2} \tag{3}$$

The impedance at point *B* is [14]

$$Z_B = Z_0 \frac{Z_A + jZ_0 \tan \beta l_g}{Z_0 + jZ_A \tan \beta l_g} = \frac{\frac{jZ_0 \tan \beta(l_d/2)}{2} + jZ_0 \tan \beta l_g}{1 - \frac{\tan \beta(l_d/2) \cdot tan\beta l_g}{2}} \tag{4}$$

Thus the T-shaped DGS can be seen as a series transmission line branch with impedance Z_B for the transmission line from Port #1 to Port #2. Hence, the S_{21} from port #1 to port #2 is [14]

$$S_{21} = \frac{2}{2 + Z_B/Z_{01}} \tag{5}$$

where Z_{01} is the characteristic impedance of the slot radiator. It can be seen in (5) that, to have high isolation (low mutual coupling) between ports 1 and 2, S_{21} should be made zero, so that Z_B becomes infinity. Thus, we make the denominator of Z_B in (4) zero, i.e.

$$1 - \frac{\tan \beta(l_d/2) \cdot tan\beta l_g}{2} = 0 \tag{6}$$

Using (6) to express l_g yields the condition for infinite Z_B

$$l_g = \frac{\arctan(\frac{2}{\tan \beta(l_d/2)})}{\beta} \tag{7}$$

which is plotted against l_d in Figure 4. The pairs of values for l_g and l_d on the curve make S_{21} at 2.45 GHz equal to zero. With l_d = 1 mm and l_g = 20.13 mm, the T-shaped DGS becomes a

simple slot in [12], which would occupy too much area on the metal cover of the smartphone. In fact, there are many possible combinations for l_g and ld, as shown in the curve of Figure 4, which can make S_{21} in (5) equal to zero. For example, with l_d = 36 mm and l_g = 4.6 mm, the design is close to the values of l_d = 34 mm and l_g = 4 mm used in our proposed dimensions shown in Table 1. The discrepancy is mainly due to the T-junction at point *A* is not taken into account and coupling between the DGS and slot radiation is neglected. However, the function of (7) or the curve in Figure 4 can provide a starting point to design the DGS for the CSMA to satisfy different Industry-Design (ID) and Mechanical-Design (MD) requirements. The width w_d of the T-shaped DGS affects the decoupling bandwidth, which will be studied later.

4. Study of the antenna

The S-parameters of the proposed antenna with different values of w_d is shown in Figure 5. It can be seen that, as w_d varies from 0.5 mm, to 1 and 1.5 mm, the impedance bandwidth (IMBW) has negligible changes, while the decoupling bandwidth increases. To make the antenna compact, we choose w_d = 1 mm, as it can provide enough decoupling bandwidth for the 2.4-GHz WLAN band. Note that as w_d increases from 0.5 mm, 1 to 1.5 mm, l_d needs to be slightly adjusted from 32.5 mm, to 34 and 35.1 mm, respectively.

To study the decoupling performance of the CSMA, we use two similar antennas, Ant #1 and Ant #2 as shown in the caption of Figure 6, for comparison. Ant #1 is a single slot antenna and Ant #2 is our proposed CSMA without having the T-shaped DGS. The dimensions of the slot radiators in Ants #1 and #2 are same as that of the proposed CSMA. The simulated S-parameters of these two antennas are compared with those of the proposed CSMA in Figure 6. It can be seen that Ant #1 resonates at 2.52 GHz with the IMBW for $S_{11} \leq -6$ dB of 2.48–2.56 GHz. Ant #2 resonates at a slightly lower frequency of 2.46 GHz, but the resonance is not strong enough to form a useful frequency band with S11 ≤ −6 dB. The mutual coupling between the input ports of Ant #2 is quite strong at $S_{21} = -7.8$ dB at the resonant frequency 2.46, which is not acceptable for MIMO systems. Figure 6 shows that the proposed CSMA

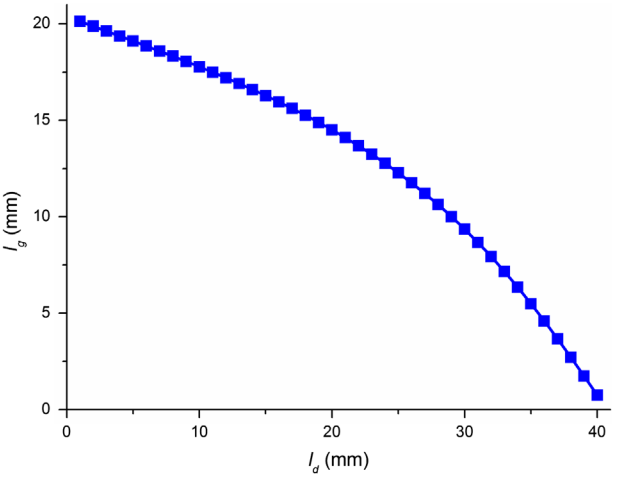

Figure 4. Relationship curve between *lg* and *ld* to satisfy $S_{21} = 0$ at 2.45 GHz.

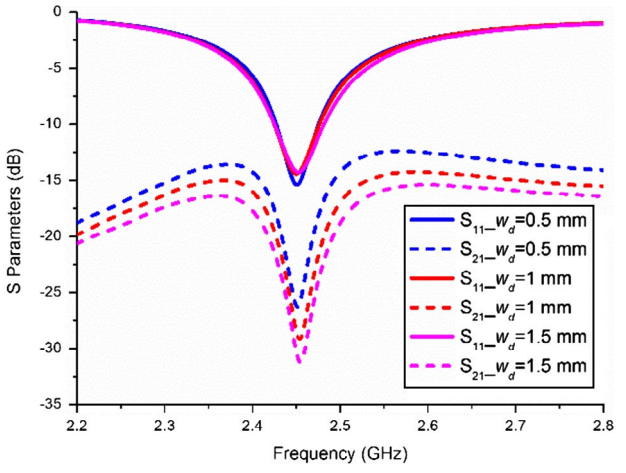

Figure 5. Simulated S_{11} and S_{21} of CSMA with different *wd*.

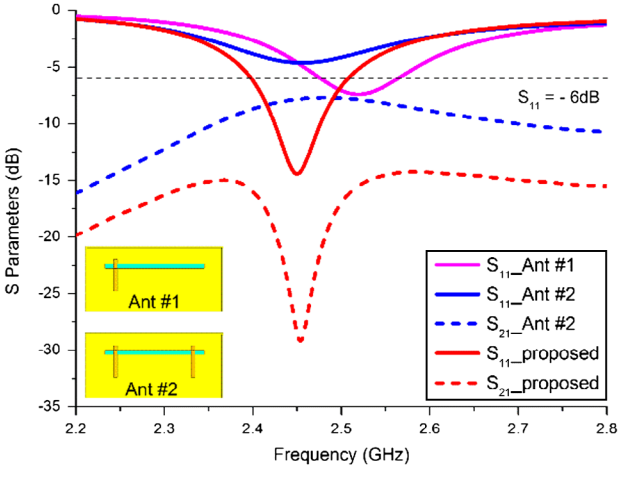

Figure 6. Simulated S_{11} and S_{21} of Ant #1, Ant #2 and proposed CSMA.

has an IMBW for $S_{11} \leq -6$ dB of 2.4–2.51 GHz, enough to cover the 2.4-G WLAN band. The decoupling bandwidth for $S_{21} \leq -15$ dB is 2.37–2.53 GHz, which is wider than the IMBW. These results show that the T-shaped DGS in the CSMA can significantly reduce mutual coupling and increase the IMBW of the antenna.

Current distribution is used to further study decoupling of the CSMA. Figure 7 shows the simulated current distribution of the antenna at 2.45 GHz. With port #1 excited and port #2 terminated with a 50-Ω load, Figure 7(a) shows that the currents are mainly concentrated on the left-hand side of the slot radiator and the T-shaped DGS. The currents on the right-hand side of the antenna remain very weak. It can be seen in Figure 7(a) that there is an obvious current null in the middle of the slot radiator. This is because Z_B, as discussed in Section II, is infinity, making the slot radiator open circuited in the middle.

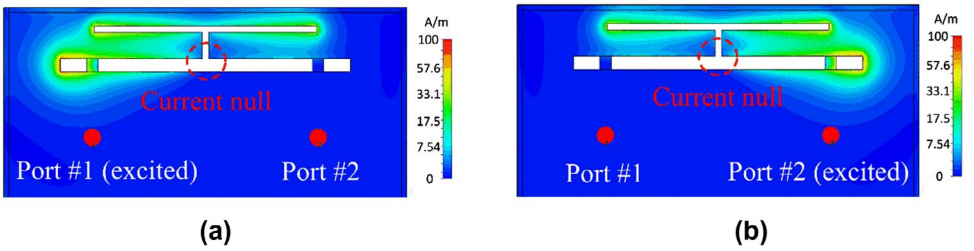

Figure 7. Current distribution at 2.45 GHz: (a) port #1 excited and (b) port #2 excited.

When port #2 is excited and port #1 is terminated with a 50-Ω load, the current distribution is shown in Figure 7(b). Due to the symmetrical structure of the antenna, the current distribution is just a mirror image of Figure 7(a).

5. Result and discussions

5.1. S-parameters

The S-parameters of the CSMA have been simulated and the prototyped antenna of Figure 2 has been measured using a vector-network analyzer Rohde & Schwarz ZVA 24. In measurement, when one port is excited, the other port is terminated with a 50-Ω load, and vice versa. The simulated and measured results are shown in Figure 8. Since the antenna has a symmetrical structure, the simulated S_{11} and S_{21} are identical to S_{22} and S_{12}, respectively, so we only show the simulated S_{11} and S_{21} in Figure 8. However, for measurement, we show S_{11}, S_{22} and S_{21} (which is same as S_{12}). It can be seen in Figure 8 that the simulated and measured results have good agreements. The measured IMBW (S_{11} and $S_{22} \leq -6$ dB) is about 2.4–2.48 GHz, enough to cover the 2.4-GHz WLAN band (2.4–2.48 GHz). Note that $S_{11} \leq -6$ dB is used here to define the bandwidth, which is normally used in mobile antenna design in industry [15]. Across the 2.4-GHz WLAN band, the simulated and measured mutual coupling levels (indicated by S21) range from −16 to −29 dB and from −19 to −29 dB, respectively, which is good enough for MIMO systems.

5.2. Radiation performance

The radiation pattern, efficiency, and realized peak gain of the CSMA have been measured using the antenna measurement equipment, the Satimo SG24 system. The simulated and measured radiation patterns of the MIMO antenna at 2.45 GHz in the x-z and x-y planes are shown in Figure 9. It can be seen in Figure 9(a) that the radiation patterns of ports #1 and #2 are complementary to each other, indicating that the proposed MIMO antenna can receive signals from different directions to provide good pattern diversity. In Figure 9(b), the radiation patterns obtained by exciting either ports are bidirectional in the ± y direction, which is typical for slot antennas.

The efficiency and realized peak gain of the CSMA are shown in Figure 10. Due to the symmetrical structure of the antenna, simulated efficiency and gain for port #1 excited

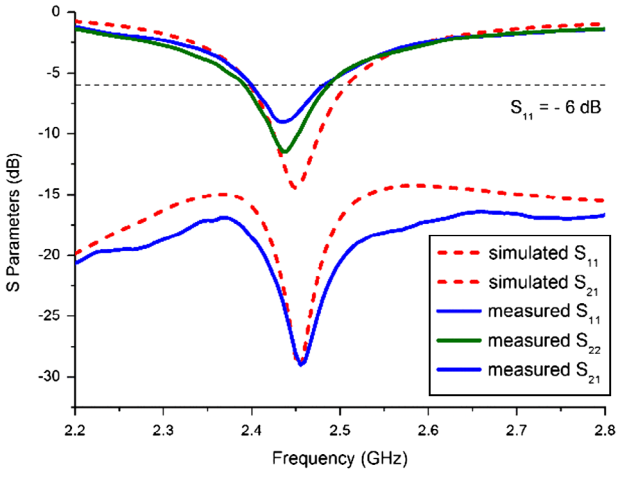

Figure 8. Simulated and measured S_{11} and S_{21} of CSMA.

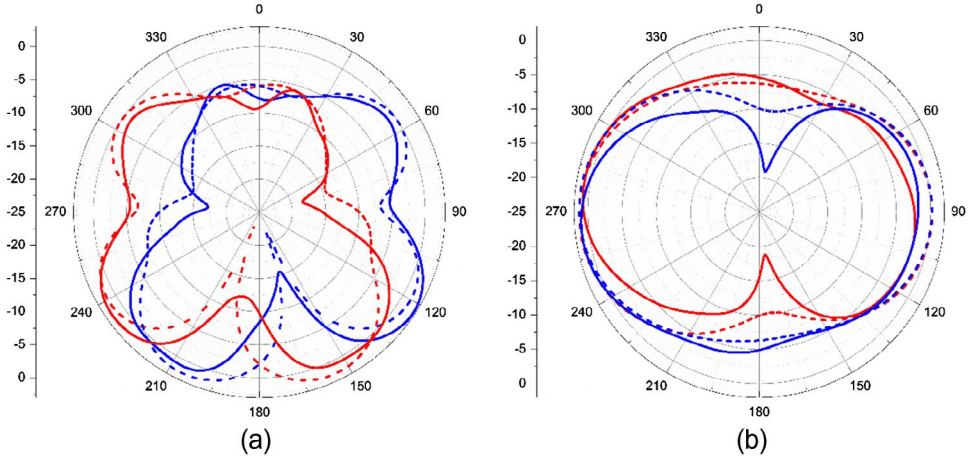

Figure 9. Simulated and measured radiation patterns at 2.45 GHz: (a) x-z plane and (b) x-y plane (- - - - simulated pattern with port #1 excited; —— measured pattern with port #1 excited; - - - - simulated with port #2 excited; —— measured with port #2 excited).

and #2 excited are identical. It can be seen in Figure 10(a) that the simulated efficiencies are 70–90% in 2.4-G WLAN band. The measured efficiencies are 58–74% and 64–77% when ports #1 and #2, respectively, are excited. Figure 8(b) shows that the simulated realized peak gain ranges from 3.55 to 4.45 dBi in the 2.4-G WLAN band. The measured realized peak gains for ports 1# and #2 excited ranges from 2.7 to 4.1 dBi and from 2.9 to 4.1 dBi, respectively. The discrepancies between simulated and measured results are mainly due to the measurement and fabrication tolerance, and the feeding cable effects in measurements [16].

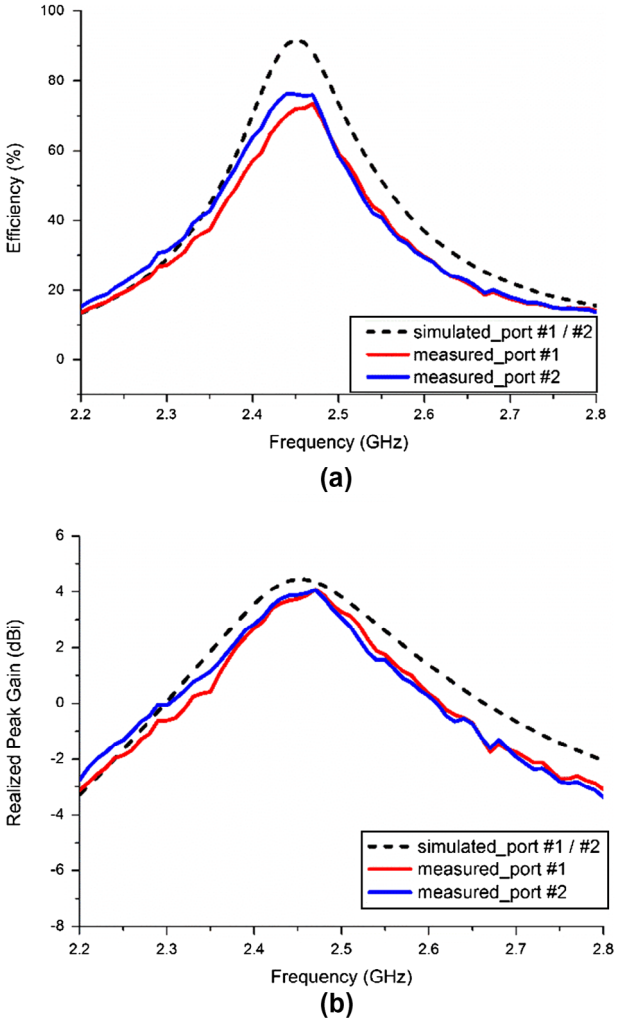

Figure 10. Simulated and measured (a) efficiencies and (b) gains of CSMA.

5.3. MIMO performance

The diversity and multiplexing performances of the CSMA are evaluated using envelope-correlation coefficient (ECC) and multiplexing efficiency, respectively, as shown in Figure 11. The ECC is obtained using the 3-D radiation pattern method in [17], and the multiplexing efficiency is calculated using the method in [18]. It can be seen in Figure 11(a) that the ECC values using the measured and simulated radiation patterns range from 0.0489 to 0.0867 and 0.00084 to 0.051, respectively. The small discrepancy in ECC results is due to the difference between using the simulated and measured radiation patterns in calculations. Figure 11(b) shows that the measured multiplexing efficiency in the 2.4-GHz WLAN band ranges from 58% to 73%, which is acceptable for practical smartphone designs [5,8].

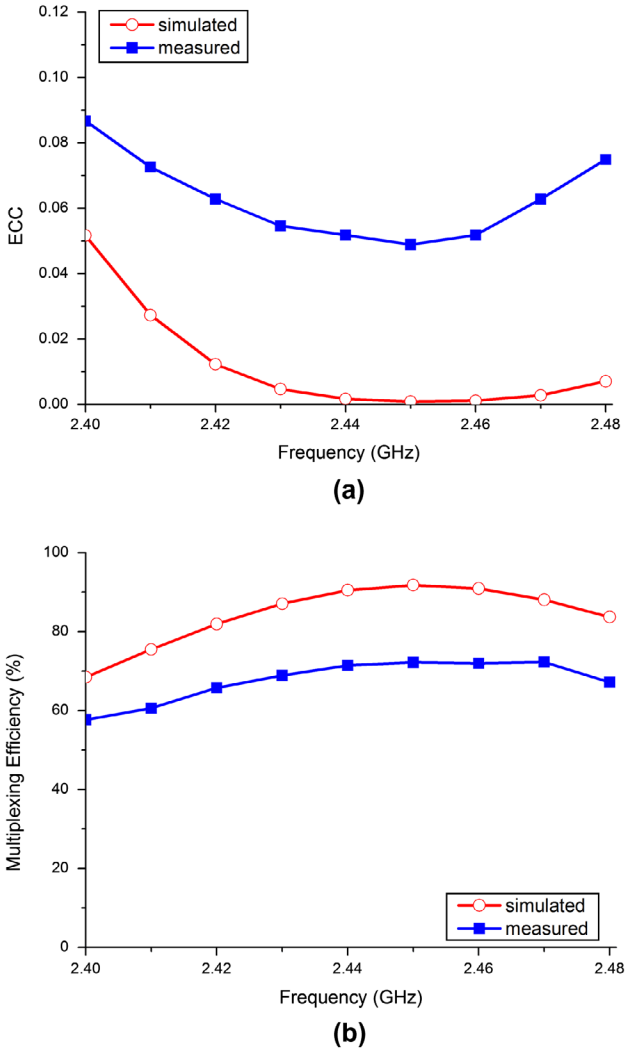

Figure 11. Simulated and measured MIMO performance of CSMA (a) ECC and (b) multiplexing efficiency.

6. Conclusions

In this paper, a CSMA for smartphones with metal housing for MIMO communication is proposed. The antenna has two input ports sharing the same slot radiator and a T-shaped DGS for reducing mutual coupling. The transmission theory is used to analyze the decoupling mechanism of the antenna. An equation has been derived to roughly select the dimensions of the T-shaped DGS for the CSMA. Measured results have shown that the antenna has an IMBW of 2.4–2.48 GHz, with mutual coupling ranging from −19 to −29 dB and the ECC below 0.0867. The results indicate that the proposed CSMA is a promising candidate for the design of MIMO antenna for smartphones with metal housing.

Disclosure statement

No potential conflict of interest was reported by the authors.

References

[1] Pascolini M, Hill RJ, Zavala J, et al. Bezel gap antennas. Google Patents; 2012.
[2] Nickel J, Zavala J, Zhou Y, et al. Multiband antennas formed from bezel bands with gaps. Google Patents; 2015.
[3] Chiang B, Springer GA, Kough DB, et al. Microslot antennas for electronic devices. Google Patents; 2013.
[4] Wong KL, Wu PR. Low-profile dual-wideband dual-inverted-L open-slot antenna for the LTE/WWAN tablet device. Microwave and Optical Technology Letters. 2015;57(8):1813–1818.
[5] Wong K-L, Tsai C-Y. Low-profile dual-wideband inverted-T open slot antenna for the LTE/WWAN tablet computer with a metallic frame. IEEE Trans Antennas Propag. 2015;63(7):2879–2886.
[6] Diallo A, Luxey C, Le Thuc P, et al. Study and reduction of the mutual coupling between two mobile phone PIFAs operating in the DCS1800 and UMTS bands. IEEE Trans Antennas Propag. 2006;54(11):3063–3074.
[7] Chen S-C, Wang Y-S, Chung S-J. A decoupling technique for increasing the port isolation between two strongly coupled antennas. IEEE Trans Antennas Propag. 2008;56(12):3650–3658.
[8] Ban Y-L, Yang S, Chen Z, et al. Decoupled planar WWAN antennas with T-shaped protruded ground for smartphone applications. IEEE Antennas Wirel Propag Lett. 2014;13:483–486.
[9] Wu D, Cheung SW, Li QL, et al. Decoupling using diamond-shaped patterned ground resonator for small MIMO antennas. IET Microwave Antennas Propag. 2017;11(2):177–183.
[10] Wu D, Cheung S, Yuk T, et al. editors. Design of a printed multiband MIMO antenna. 2013 7th European Conference on Antennas and Propagation (EuCAP); IEEE; 2013.
[11] Li J-F, Chu Q-X. A compact dual-band MIMO antenna of mobile phone. Journal of Electromagnetic Waves and Applications. 2011;25(11–12):1577–1586.
[12] Chiu C, Song S, Murch RD. Complementary two-port antennas with low mutual coupling. IET Microwave Antennas Propag. 2012;6(2):135–141.
[13] Booker HG. Slot aerials and their relation to complementary wire aerials (Babinet's principle). J Inst Electr Eng -Part IIIA: Radiol. 1946;93(4):620–626.
[14] Pozar DM. Microwave Engineering. 3rd ed. Wiley; 2005.
[15] Wong K-L. Planar antennas for wireless communications. Microwave J. 2003;46(10):144–145.
[16] Liu L, Cheung S, Weng Y, et al. Cable effects on measuring small planar UWB monopole antennas. Ultra wideband-current status and future trends. InTech; 2012.
[17] Knudsen MB, Pedersen GF. Spherical outdoor to indoor power spectrum model at the mobile terminal. IEEE J Sel Areas Commun. 2002;20(6):1156–1169.
[18] Tian R, Lau BK, Ying Z. Multiplexing efficiency of MIMO antennas. IEEE Antennas Wirel Propag Lett. 2011;10:183–186.